# Dependence of mechanical properties of polyamide components on build parameters in the SLS process

# Dependence of mechanical properties of polyamide components on build parameters in the SLS process

B. Caulfield, P.E. McHugh, S. Lohfeld*

National Centre for Biomedical Engineering Science
and Department of Mechanical and Biomedical Engineering,
National University of Ireland, Galway, Ireland
* *Corresponding author, Email:* Stefan.Lohfeld@nuigalway.ie, *Phone:* +353-91-492963, *Fax:* +353-91-494596

Accepted Manuscript. Published version: http://dx.doi.org/10.1016/j.jmatprotec.2006.09.007

## Abstract

Customised properties of parts manufactured using the selective laser sintering process are achievable by variation of build parameters. The energy density, controlled by laser power, distance between scan lines and speed of the laser beam across the powder bed, all have a very strong influence on the density and the mechanical behaviour of the parts. The present paper investigates the influence of the energy density on physical and mechanical properties of parts produced using polyamide. Additionally, the effect of part orientation during the build is examined. Knowledge of the influence of these parameters allows one to establish trendlines which link build settings to resulting part properties, and hence to fabricate customised parts with predetermined properties.

Keywords: Solid freeform fabrication, Selective laser sintering, Energy density, Part orientation, Properties.

## 1 Introduction

Solid freeform fabrication (SFF) techniques have been developed for industrial and engineering use. Traditionally, these techniques have been focused in the area of rapid prototyping where the primary interest was in generating a physical model of a component or system for visualisation purposes or to explore kinematic functionality, in the case of a mechanism with moving parts, for example. More recently, rapid prototyping has evolved to become rapid manufacturing where SFF techniques are being used to produce finished (or at least near finished) components.

The mechanical properties of produced parts are important in the area of rapid prototyping, in that the prototype must have sufficient mechanical integrity and surface quality for handing and demonstration purposes. Mechanical properties become critically important in the area of rapid manufacturing where the stiffness, strength, and surface finish must be sufficient to meet in-service loading and operation requirements, and where they must be comparable to those produced using traditional manufacturing routes to make the SFF based processes competitive.

In addition to general engineering, SFF techniques have readily found applications in medicine. Computed Tomography (CT) scan data has been used to produce physical models of anatomical structures; such models can be classified as physical biomodels using the definitions in [1]. Indeed producing three dimensional physical biomodels with complex geometries layer by layer can be viewed as effectively an inversion of the CT scanning process. Models of bone structures or other body tissues have proven to be very helpful in diagnostics, pre-operation planning and implant design [2, 3].

In biomedical engineering, which involves a combination of engineering and medicine, these physical biomodels, mostly derived from bone structure, are utilised for mechanical tests and validation of computational models [1]. The advantages of using such models of bone are obvious: unlimited replication of the same architecture, elimination of biological variability of tissue properties, and the elimination of the necessity for tissue donors.

There is a variety of SFF processes, for example Stereolithography (SLA), Selective Laser Sintering (SLS), Fused Deposition Modelling (FDM), and 3-Dimensional Printing (3DP) [4-7]. For bone models, surgeons typically prefer models generated using the SLS process, which are usually made from polyamide/nylon, because they look and feel very similar to bone [4]. This material also has properties similar to those of real bone, which makes it a good choice to produce physical test models.

However, mechanical properties of the produced part are not solely controlled by the base material itself. They are also influenced by the production process. The present paper focuses on the SLS process. As SLS is a process in which powder particles are fused or sintered together by heat supplied by a laser, the part density strongly depends on the degree of sintering. This again depends on the energy density of the laser as well as on several other factors, which will be discussed in detail later on. These parameters influence the mechanical behaviour of a produced part [8]. While in most cases parts will be produced using predetermined settings for "best" results, one may also have an interest in achieving variations in part properties. This can be in terms of having different parts with different properties, or a spatial variation in properties within a single part. To produce parts with customised properties using SLS, the three factors laser power, scan spacing (the distance between two laser scan lines when sintering an area), and part orientation appear most important.

Even though the mechanical properties of the produced part are of significant importance, in particular in the rapid manufacturing area, very little has been reported in the literature on studies performed to measure mechanical properties for material processed using SFF techniques, and the SLS process in particular. Ho et al. in 1999 [8] reported on the effects of energy density on morphology and properties of polycarbonate processed by SLS, and Casalino et al. in 2005 [9] reported on the properties of sand moulds for casting prepared by SLS. Effects of process parameter settings on the properties of parts manufactured using techniques similar to SLS can be found elsewhere [10-12]. However no such studies have been reported for polyamide, processed using the SLS technique.

## 2 Objectives

As stated above, the present work is focused on the SLS process. The specific material of interest is polyamide. The paper reports on the effects of varying the energy density, generated by the laser, on the physical and mechanical properties of produced specimens. The energy density is varied by changing the laser power at a fixed value of laser scan spacing. Knowing the relationship between SLS parameter settings and material properties will make it possible to manufacture parts with predetermined properties, customised for various applications. In addition to energy density, the influence of the build orientation is explored because it is expected that this will have a significant influence on the material behaviour. Due to the layer-by-layer manufacturing process, orthotropic behaviour is a possibility if the fusion between two successive layers is different from the fusion within one layer.

## 3 The SLS process

Selective Laser Sintering is a process where a laser beam acts on a preheated powder bed to liquefy (either partially of fully) and fuse the powdered material. The sintering is performed in a selected region on the powder bed that corresponds to a slice through the three dimensional geometry of the part being produced. Each time a slice is finished, the build chamber is lowered and new powder is spread from a feed chamber over the previous layer. This way, parts are build up layer by layer. The sintered areas, and eventually the parts themselves, are supported by surrounding powder and there is no need for additional support structures such as those used in SLA and FDM.

The major build parameters in the SLS process are a) supplied energy density, b) part build orientation, c) feed/part bed temperatures, d) layer thickness, e) temperature rates/ramps, f) powder consistency, and g) material type. Both the supplied energy density and the part build orientation are part dependant, i.e. these parameters can be different for each part in any one build. Many of the other build parameters are build dependant, or more precisely layer dependent, i.e. the parameters are the same for all parts within a single layer of a build. These parameters can be changed with the build height.

The supplied energy density (ED) level is a measure of the amount of energy supplied to the powder particles per unit area of the powder bed surface. It is a function of three laser components – laser fill power (LP), laser fill scan spacing (SS) and laser beam speed (LS). Based on J. C. Nelson's definition of the ED of the laser onto the powder bed [13], this function is described through equation (1)

$$ED = \frac{LP}{SS \times LS} \tag{1}$$

with LP units in Watt, SS units in mm, and LS units in mm/s. The ED therefore is measured in J/mm².

The part build orientation is defined as the orientation of the major axis (axis along the longest dimension) of the part relative to the top plane of the powder bed. The relationship between part orientation in the build chamber and part properties can be examined by isolating this parameter from the others.

# 4 Experimental

All parts were manufactured on a DTM Sinterstation 2500$^{plus}$ using DuraForm$^{TM}$ Polyamide powder (3D Systems). The installed control software for the Sinterstation was version V3.100 of "Sinter". Directions in the build chamber are as follows: the x-axis is parallel to the front of the machine, while the y-axis is perpendicular to this. The top plane of the powder bed is then the x-y-plane of the build chamber. The z-axis is perpendicular to the x-y-plane.

Test specimens were designed to the ASTM D638-00 standard. The most important dimensions of this 'dog-bone' shaped specimen are summarised in Figure 1.

While the laser power was varied, the laser fill scan spacing was kept fixed at 0.15 mm. The batch was divided into two groups of different part build orientations. The parts in group 1 were orientated at 0° (longest axis built parallel to the x-axis), group 2 parts were orientated at 90° (longest axis build parallel to the z-axis) (**Figure 2**). Each group contained seven lots produced at seven different energy density levels and each lot with seven specimens. This resulted in a total of 49 specimens each, for the 0° and for the 90° build orientations.

The laser beam speed (speed at which the laser beam spot on the powder bed is moved along the x-axis of the build chamber) was fixed at 5080 mm/s. The energy densities applied to the lots were calculated using equation (1) and are given in **Table 1**.

All parts were built without applying scale factors for compensation of the inherent shrinkage during cooling. After production the samples were removed from the part cake and cleaned manually. Sandblasting and pressurised air were used to remove remnants of the powder. The dimensions of the specimens were obtained using callipers. Each dimension was taken three times and an average of these values was associated with each part. The density of the material was found by building density specimens under the same build conditions as the tensile specimens. The density specimens were small square prisms of intended dimensions 50 mm × 50 mm × 3 mm. Once the density specimens were built, their dimensions were determined manually and they were weighed. Subsequently, the apparent density was found by dividing mass by volume.

Mechanical properties were determined from tension tests (ASTM D638-00) using an Instron 8874 Servo-hydraulic Biaxial Testing System. The strain was measured using a ME46-350 Video Extensometer System (Messphysik, Austria). Stress-strain diagrams (engineering stress – engineering strain) were used to identify Young's modulus, yield

strength, fracture strength and elongation at break. The stress-strain-curves also allowed one to make statements about whether or not the material's behaviour was isotropic.

# 5 Results

## 5.1 Part dimensions

All of the tensile test specimens were designed to the same dimensional specifications given in the previous section. To investigate the role the ED had on the dimensions of the test specimens, two different measurements of the specimens were taken; width and thickness. Three individual measurements of each were taken and an average value was then generated for each specimen. A sample size of six was used for each lot. An average value for the part width/thickness per ED value was generated from the recorded data. These average values were then used to develop a Cross-Sectional-Area (CSA) value for each lot. These CSA values were required when it came to creating the stress-strain diagram for each test specimen.

Once the experimental data points for each dimension had been established, a trendline was fitted to the data points. This trend could then be used to relate the specimens' dimensions to any ED level within the tested ED range.

At both orientations the part width increased with increasing energy density (see **Figure 3**). The parts build at 90° orientation were closer to the desired part width of 13 mm. All parts were smaller than intended due to shrinkage during cooling of the parts. The variation in the widths between orientations may have been due to a difference in build accuracy in the horizontal (within a layer) and vertical (perpendicular to a layer) directions for the SLS process. In addition, part shrinkage on cooling may have been different between horizontal and vertical directions.

The trendline equations applied to the experimental width data for the two build orientations are given in **Table 2**, with the x value representing the ED level and the y value representing the part width.

**Figure 4** shows that unlike the part width, the desired thickness of 3 mm was reached and exceeded by the majority of the parts. A steep increase appeared in the thickness of the 0° orientated parts with an increasing ED level. The thickness of the 90° orientated parts also increased as the ED level rose, but at a lower rate. Similar to the situation for the part widths, the variation in the dimensions with change in the build orientation could have been due to differences in the build accuracy and shrinkage between the horizontal and vertical directions for the SLS process.

The trendline equations for the thickness values as functions of the ED levels for both build orientations are given in **Table 3**, with the x values representing the ED level.

The cross sectional area (CSA) value was developed from the average part thickness and width per lot. The CSA of the part is important as it is required in calculating the stress. The intended CSA for all the parts was 39 mm². The calculated values are listed in Table 4. It is clear that at low ED levels the values were smaller, and at higher ED levels greater than the intended value.

## 5.2 Apparent Density

The density increased with increasing ED level (see **Figure 5**). This can be explained by the fact that higher ED levels cause a better fusion of the powder particles, resulting in a

more solid part being formed. For the parts orientated at 0° the density was consistently higher than that achieved for the parts orientated at 90°.

### 5.3 Mechanical Properties

A comparison of the stress-strain curves obtained for parts built at various ED levels revealed a rather brittle behaviour for parts built at low ED levels (see **Figure 6**). When sintering at higher ED levels the bonds between the powder particles become stronger, which leads to a more ductile behaviour with large plastic regions in the stress-strain curves.

For the parts built at the higher ED levels, it was observed that the 0° orientated parts showed a higher strength and modulus relative to the 90° orientated parts (not documented here), but the elongation at break for both orientations was very similar. Looking at the effect of the ED on the stress-strain curves of the specimens, as presented in **Figure 6**, it is clear that as the ED level increased so did the Young's modulus and the elongation at break.

### 5.4 Young's Modulus

On the basis that the thickness of the specimen (t) was smaller than the width (w) and the length (l) it was assumed that the specimen behaved as a 2D orthotropic material in plane stress, in the plane of the specimen shown in **Figure 2**. As a result, two directional moduli were determined, $E_1$ and $E_2$. The subscripts denote the assumed principal material axes: 1 parallel to the layer direction and 2 perpendicular to the layer direction. $E_1$ was found by applying a tensile stress along the major axis of the 0° orientated specimens. $E_2$ was found in the same way, however the tests were performed on the 90° orientated specimens. These two tensile test configurations are summarised in **Figure 7**. In this model the lines mark the interfaces of the sintered layers.

A sample size of six tensile specimens per lot was used. The stress was calculated using the average CSA value for each lot. The resulting stress-strain curve was used to find the corresponding Young's modulus. The moduli results were tabulated and plotted against the ED level used to create the specimens and a trendline was then fitted to these data points.

From **Figure 8** it can be seen that there was a difference between the 0° and 90° orientated parts, with the 0° parts having higher Young's modulus values along the tested ED range. The 90° orientated parts had a tighter spread of data points relative to the 0° orientated parts. There also was a difference of up to 500 MPa in the Young's modulus values of the 0° orientated parts across the ED range. Therefore, it is evident from examination of the data presented in **Figure 8**, that the ED level used to create the parts had a strong influence on the resultant Young's modulus value, which can be related back to the density of the parts. As the density of the part increases so does the modulus; in fact there is a strong similarity between the shape of the curves in **Figure 8** and the density curves shown in **Figure 5**.

### 5.5 Yield Strength

As for Young's modulus, the yield strength was measured from specimens of both build orientation, giving $Y_1$ for 0° orientated specimens and $Y_2$ for 90° orientated specimens. From **Figure 9** it is clear that the $Y_1$ values for the 0° orientation build across the tested ED range were greater than the $Y_2$ values for the 90° orientation build, with the only exception being at the highest ED level of the tested range. The $Y_2$ values exhibited a greater dependence on the ED level than the $Y_1$ values. In general yield strengths increased with an increase in ED.

### 5.6 Fracture Strength

The 0° orientated parts had a greater fracture strength than the 90° orientated parts along almost the entire tested ED range (see **Figure 10**). It can also be seen that in general the fracture strengths for both orientations increased with the ED level, except for the highest ED level.

### 5.7 Elongation at Break

The elongation at break was higher for the 90° orientated parts for almost the entire tested ED range (see **Figure 11**). The values increased significantly for both orientations with an increasing ED level, except for the highest ED level.

### 5.8 Material Morphology

An investigation into the material morphology of the produced specimens was carried out. This investigation involved examination of the physical construction of the SLS produced parts at a microscopic level. This investigation was intended to help explain why the ED level plays a key role in the determination of the material properties. In addition to the microstructural morphology, the macroscale fracture modes of the specimens during tensile testing were assessed.

**Figure 12** shows a sample surface of four of the test specimens built at 0°. The LP used in their creation is shown beneath each picture. The 0° orientated specimens were used so as to examine the surface of the individual layers. The surface of the specimen built under an LP of 9 W was porous. These pores are formed when certain powder particles receive an insufficient ED level resulting in poor fusion of these particles to surrounding particles. These particles become detached from the surface of the layer leaving the voids. As the ED level increased the voids in the surface began to fade and the surface became smoother (see the 15 W picture). As the LP increased beyond 15 W the surface quality seemed to deteriorate giving an increasingly rougher texture. This degradation possibly occurred due to excessive exposure of the laser to the powder causing the particles to burn (see 18 W and 21 W pictures).

**Figure 13** shows a close-up of the layers in some test specimens built at various laser powers. In order to examine the layers in this way the specimens chosen for examination had to be built with their surface perpendicular to the horizontal plane, i.e. the 0° build orientation. This allowed the layers to be identified easily, especially at low ED levels (see 9 W (c)). As the magnification of the SEM is increased the make up of the layers can be examined. 9 W (a) shows three individual layers; both these and the interlayer regions can be clearly identified. It can be seen that the powder particles are characteristically fused together within one layer but the fusion between adjoining layers is not as defined. The method behind the construction of the parts in the SLS is evident in the SEM images of the test specimens built under an LP of 11 W and 13 W shown in **Figure 13**. This, visually, supports the assumption that the SLS parts can be considered to be multi-layered structures.

With the lower LP values, defects and relatively large gaps were present between the layers. As the LP increased the amount of defects between the layers decreased but the layers were still visible. At an LP of 18 W the layers became undefined and were fully fused together to give a more defined solid (see 18 W picture). With a further increase in ED, the recognition of the layers disappeared.

The fracture surfaces shown in Figure **14** confirm the findings in respect of the layer morphology. At the lowest ED level the powder particles within the parts were loosely bound and the majority of the particles could be recognised individually. Only a low fraction of the particles had liquefied, therefore their spherical shape can still be easily seen (see 6 W picture). This also led to a rough fracture surface. As the ED level increased, fusion of the powder particles increased and they became harder to be independently identified. From the fracture surface of the specimen built under an LP of 9 W it can be seen that the fusion of the particles does not seem to be uniform; large areas were fused together with other areas showed little fusion resulting in the appearance of defects and voids. This could explain the relatively low strength of the specimens built under the low ED levels. At the highest ED levels the fracture surfaces were comparatively smooth.

The fracture surfaces of the parts revealed how the ED affected the material morphology. By looking at the morphology of parts built under an LP of 6 W (**Figure 14**) it is clear that the surface is rough and uneven. If a comparison is made between this microstructure and the macrostructure of the fracture surface one would expect to see a jagged fracture. This is indeed seen in the actual fracture of the test specimen, as shown in **Figure 15**.

**Figure 16** shows the fracture of the specimen built under an ED level of 0.01706 J/mm², an LP of 13 W and an SS of 0.15 mm, it can be seen that the fracture line of the specimen is quite horizontal.

### 5.8.1 Composite Material Fracture Perspective

Prior to testing the specimens a prediction of the fracture characteristics can be made. The assumption is that the orientation of the specimens will affect the fracture, especially if the specimens are assumed to consist of a multi-layered orthotropic material.

If a specimen built at 0° is tested to fracture one would expect the fracture surface to be jagged. This is because the stress is applied along each of the layers of the specimen. It is assumed that each of the layers has exactly the same mechanical properties but by examining the microstructure of the layers it is clear that small defects and voids are present in each of the layers. These defects would inevitably affect the strengths of each of the layers. As the stress builds up along the layers each will fracture at different areas of weakness, thus resulting in a jagged fracture.

**Figure 17** shows a 0° orientated fracture test specimen with reference lines drawn in to illustrate the layer orientation and also shows how the expected characteristics of the fracture surface of the specimen. This theoretical fracture is seen in reality in **Figure 18**.

The fracture of the 90° orientated specimens should appear perpendicular to the direction of the force, as this is the orientation of the layers (see **Figure 19**). Indeed, the fracture surface of the test specimen (**Figure 20**) followed the predicted pattern as shown in **Figure 19**.

From the experimental observations it can be said that the multi-layered material-like fracture of the specimens seems to occur at the lower ED levels for both orientations. As the ED level increases the fracture mode of the specimens becomes less orientation dependent and hence more isotropic.

# 6 Discussion

Equations for a selection of the trendlines shown in the previous plots (Figures 8, 9, 10, and 11) are given in Table 5. These equations are useful in that they allow for the material properties of parts to be estimated prior to their construction based on the ED level to be used to create the parts.

The part dimensions increased with an increasing ED level in all cases regardless of the build orientation. The 90° orientated parts have greater width values and were closer to the desired width value of 13 mm. However, the desired width was not reached due to shrinkage of the material during cooling. For part thickness, again the 90° orientated parts had the most accurate values. Unlike the part widths, the thickness values reached and exceeded their desired values. These results pose an interesting question as to why the accuracy depends both on the part build orientation and ED level. The increase in part dimensions as related to the ED level may be explained by the following: as the ED level increases the amount of conduction through the powder will be larger and will therefore cause excess powder particles to melt and fuse, resulting in extra width/thickness. The increase in ED may also cause the part density to increase which will cause less shrinkage within the part on cooling. The role of the build orientation and the part dimensions may be more complicated than the influence of the ED level. The 90° orientated parts were more accurate than the 0° orientated parts. In the Sinterstation build chamber the 90° orientated parts have their width and thickness dimensions controlled by the laser, whereas the 0° orientated parts have only their thickness dimensions controlled by the laser with the width controlled by the powder layer height. From this it could be argued that the dimensions controlled by the laser are more accurate than dimensions controlled by the layer height. This may be because swelling or heat conduction long the x-y-plane of the build chamber is less than in the z-direction.

The main trend seen regarding the part densities is that they increased as the ED level increased. There also seems to be a difference between the density of the parts depending on the build orientation. The 0° orientated parts showed higher densities in comparison to the 90° orientated parts. This can be attributed to the fact that the 0° orientated parts had a greater area acted on by the laser in each layer. As the laser pass will cause better fusion of the particles in this plane, these parts were generally more dense.

There are a number of main trends that were observed:

1. Both $E_1$ and $E_2$ are seen to increase with an increase in the ED level, except for the highest ED level.
2. $E_1$ is greater than $E_2$ along the tested ED range.
3. The difference between $E_1$ and $E_2$ reduces as the ED level increases.
4. Both $Y_1$ and $Y_2$ increase with an increase in the ED level, except for the highest ED level.
5. $Y_1$ is greater than $Y_2$, except at the highest ED level.
6. Large difference between $Y_1$ and $Y_2$ at lower ED levels.
7. Both of the Fracture Strengths along the 1-axis and 2-axis increase with an increase in the ED level, except for the highest ED level.
8. 0° orientated parts have a greater Fracture Strength value than the 90° orientated parts.
9. The Elongation at Break increases for both build orientations with an increasing ED level, except for the highest ED level.
10. 90° orientated parts show a greater Elongation at Break values over the 0° orientated parts.

The increase in material property values with increase in ED correlates with the corresponding increase in material density.

The difference between $E_1$ and $E_2$ is a logical consequence of the multilayered structure of the material, with the Young's modulus being greater along the primary axis in comparison to the secondary axis. This, as well as the difference between $Y_1$ and $Y_2$, shows that the material is anisotropic in nature. However, the level or degree of anisotropy decreased as the ED level increased. Better fusion of the layers accounts for the small difference between $E_1$ and $E_2$ and $Y_1$ and $Y_2$, respectively, at high ED levels, and as a consequence the parts are becoming more isotropic. The fracture strength of the 0° orientated parts in relation to that of the 90° orientated parts corresponds to what was found for Young's modulus and yield strength.

The increase in the elongation with increase in ED level can be again attributed to the increase in part density and particle fusion. Enhanced material integrity and more complete local interparticle bonding clearly results in a reduction in material brittleness. The elongation results with respect to variation in the build orientation exhibit an interesting trend, opposite to what is seen for stiffness and strength, with the 90° orientated parts having a greater elongation at break in comparison to the 0° orientated parts. This could be suggesting that the material between the layers can deform more easily that the material in the layers, which is densified to a greater degree. For the 90° orientation most of the deformation could be taken up by this inter-layer material resulting in greater overall specimen elongation, in comparison to the 0° orientation where overall specimen elongation is directly dependent on the deformation of the stiffer and denser layers themselves.

At ED levels at the top of the tested range the rate of increase of the strength and modulus values begins to decrease and in some cases the property values begin to drop. This can be attributed to the powder particles becoming damaged or burnt by excess heat from the laser, as observed from SEM micrographs. This burning will cause the material properties to deteriorate to a certain degree. The damage is only on a small scale for the samples discussed, but it is expected that it will be more severe when the ED level is increased to values above the tested range.

The general dependence of the mechanical response on the build orientation, and the increased isotropic nature of the material as the ED level is increased, is backed up by SEM observations of the material microstructure and fracture surfaces. SEM micrographs showed that the microstructure, in particular the interlayer region, changed significantly with a change in ED.

# 7 Conclusion

This study revealed that the ED level has a significant effect on the resulting material properties of the parts produced in the Sinterstation. The relationship between the ED level and a given material property described through an equation is considered to be a good representative guide for estimating the material property value for any DuraForm™ polyamide part. In some cases the experimental data exhibit a larger scatter, but the standard deviation in many cases is approximately 3 to 8 %. With these variations present the equation may not be solely sufficient to definitively predict the material properties of the parts. To address this, a recommendation for future production is to build a sample part with every build and find the material properties of this part, which then can be used to compare with (and adjust if necessary) the properties estimated by the material equation. By examining the material properties as they relate to the ED level it was observed that at lower ED levels the parts are porous, weak and anisotropic, but become more isotropic, solid and stronger as the ED level increases. As a result, it is recommended that no parts should be built under an ED level of 0.012 J/mm² unless a porous structure is required. The manufacturing of the functional parts can now be optimised so as to ensure that the required properties of a part can be 'imprinted' into the

material through the use of appropriate build parameters, i.e. ED or part build orientation. As the build parameters can be applied per layer the part can also be further customised through varying these build parameters along the z-direction. This can help in the creation of a tailor made part with the most appropriate properties for its desired function.

# 8 References


1. S. Lohfeld, V. Barron, and P.E. McHugh, *Biomodels of Bone: A Review.* Annals of Biomedical Engineering, **33**(10):1295-1311.
2. K.L. Chelule, T.J. Coole, and D.G. Cheshire. *Fabrication of Medical Models from Scan Data via Rapid Prototyping Techniques*. in *Proceedings of the TCT (Time-Compression Technologies) Conference & Exhibition*. 2000. Cardiff, UK.
3. P.S. D'Urso and M.J. Redmond, *A method for the resection of cranial tumours and skull reconstruction.* British Journal of Neurosurgery, **14**(6):555-559.
4. E. Berry, J.M. Brown, M. Connell, C.M. Craven, N.D. Efford, A. Radjenovic, and M.A. Smith, *Preliminary experience with medical applications of rapid prototyping by selective laser sintering.* Medical Engineering & Physics, **19**(1):90-96.
5. C.X.F. Lam, X.M. Mo, S.H. Teoh, and D.W. Hutmacher, *Scaffold development using 3D printing with a starch-based polymer.* Materials Science and Engineering: C, **20**(1-2):49-56.
6. W. Palm, *Rapid Prototyping Primer*, Pennsylvania State University, University Park, Pennsylvania: The Learning Factory, 2002. Available on http://www.me.psu.edu/lamancusa/rapidpro/primer/chapter2.htm
7. R. Petzold, H.-F. Zeilhofer, and W.A. Kalender, *Rapid protyping technology in medicine - basics and applications.* Computerized Medical Imaging and Graphics: the Official Journal of the Computerized Medical Imaging Society, **23**(5):277-284.
8. H.C.H. Ho, I. Gibson, and W.L. Cheung, *Effects of energy density on morphology and properties of selective laser sintered polycarbonate.* Journal of Materials Processing Technology, **89-90**:204-210.
9. G. Casalino, L.A.C. De Filippis, and A. Ludovico, *A technical note on the mechanical and physical characterization of selective laser sintered sand for rapid casting.* Journal of Materials Processing Technology, **166**(1):1-8.
10. P. Fischer, V. Romano, H.P. Weber, N.P. Karapatis, E. Boillat, and R. Glardon, *Sintering of commercially pure titanium powder with a Nd:YAG laser source.* Acta Materialia, **51**(6):1651-1662.
11. Y. Tang, H.T. Loh, Y.S. Wong, J.Y.H. Fuh, L. Lu, and X. Wang, *Direct laser sintering of a copper-based alloy for creating three-dimensional metal parts.* Journal of Materials Processing Technology, **140**(1-3):368-372.
12. T. Friedel, N. Travitzky, F. Niebling, M. Scheffler, and P. Greil, *Fabrication of polymer derived ceramic parts by selective laser curing.* Journal of the European Ceramic Society, **25**(2-3):193-197.
13. J.C. Nelson, *Selective Laser Sintering: A definition of the process and an empirical sintering method.* PhD dissertation, 1993, University of Texas: Austin.

# 9 Acknowledgements

The authors acknowledge support from the Programme for Research in Third Level Institutions (PRTLI), administered by the Higher Education Authority.

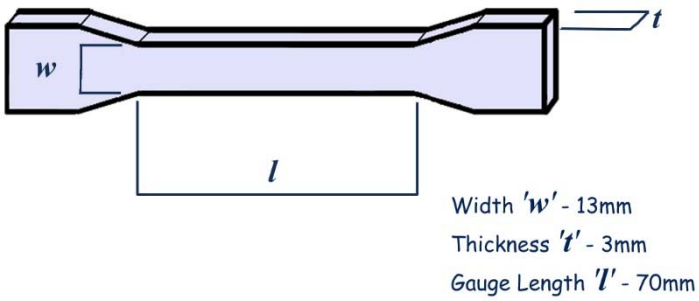


Width 'w' - 13mm
Thickness 't' - 3mm
Gauge Length 'l' - 70mm

Figure 1: Dog-bone tensile test specimen

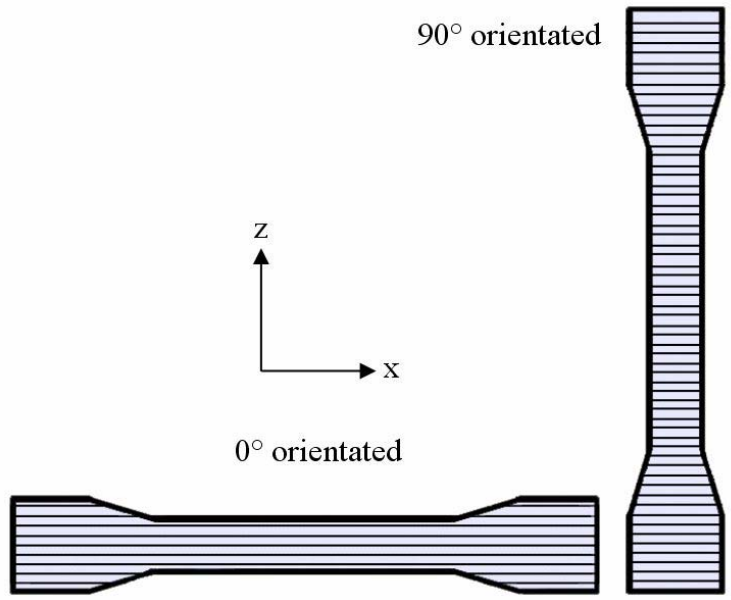


Figure 2: Part build orientations. Black lines indicate layer interfaces.

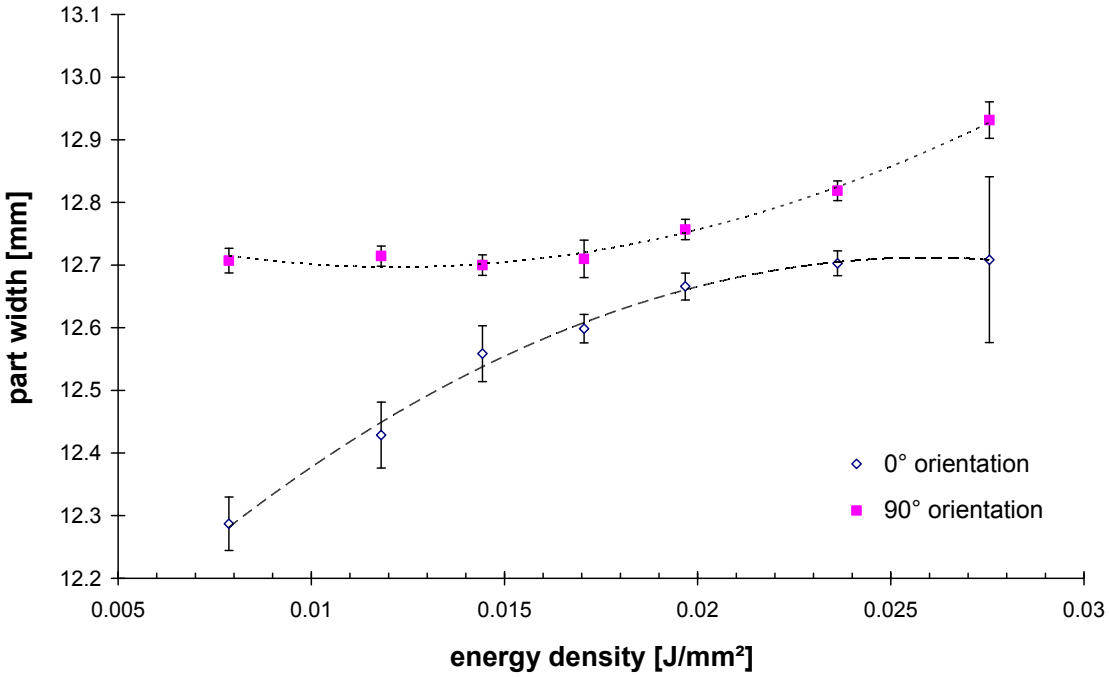


Figure 3: Part width comparison. Error bars indicate the standard deviation within each set of samples.

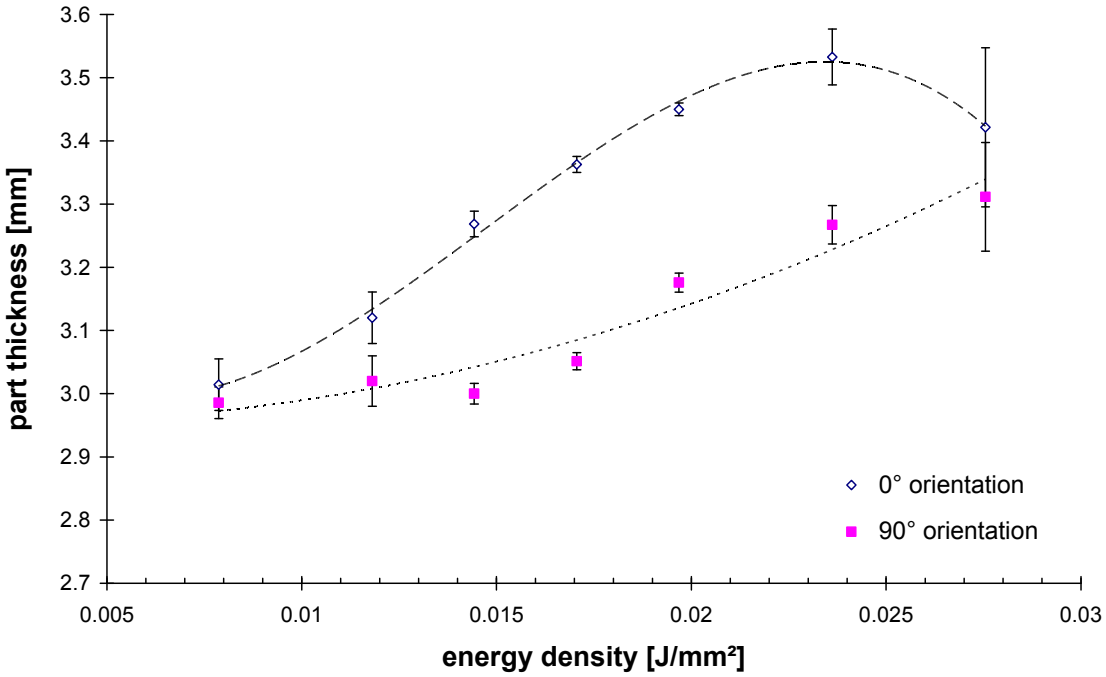


Figure 4: Part thickness. Error bars indicate the standard deviation within each set of samples.

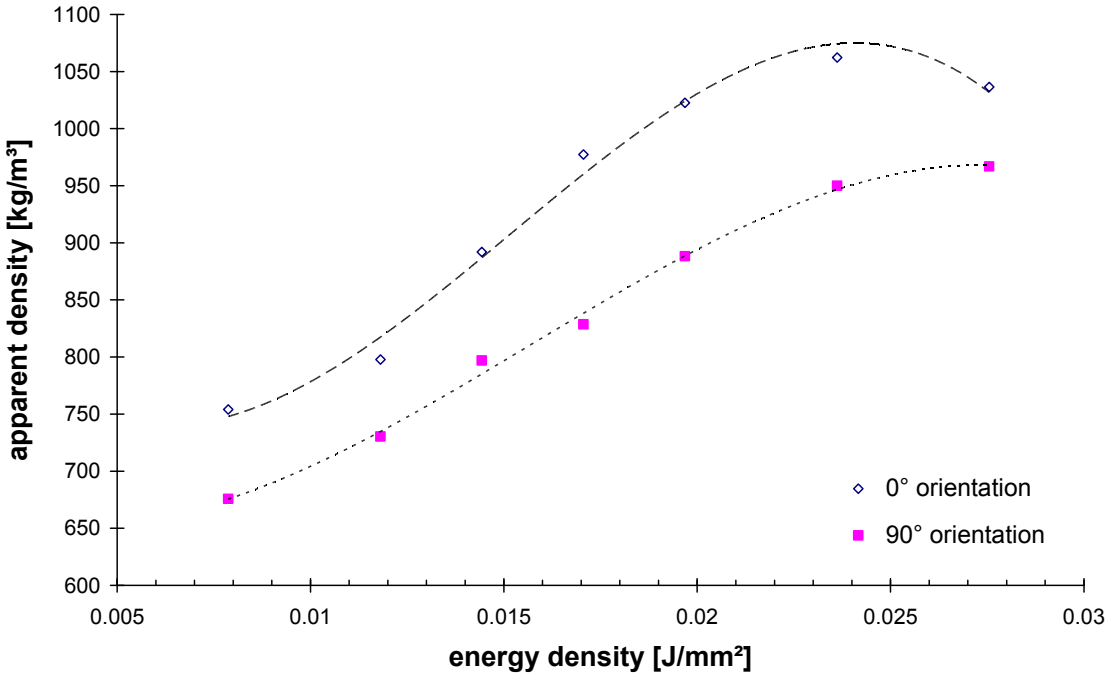


Figure 5 : Part density comparison

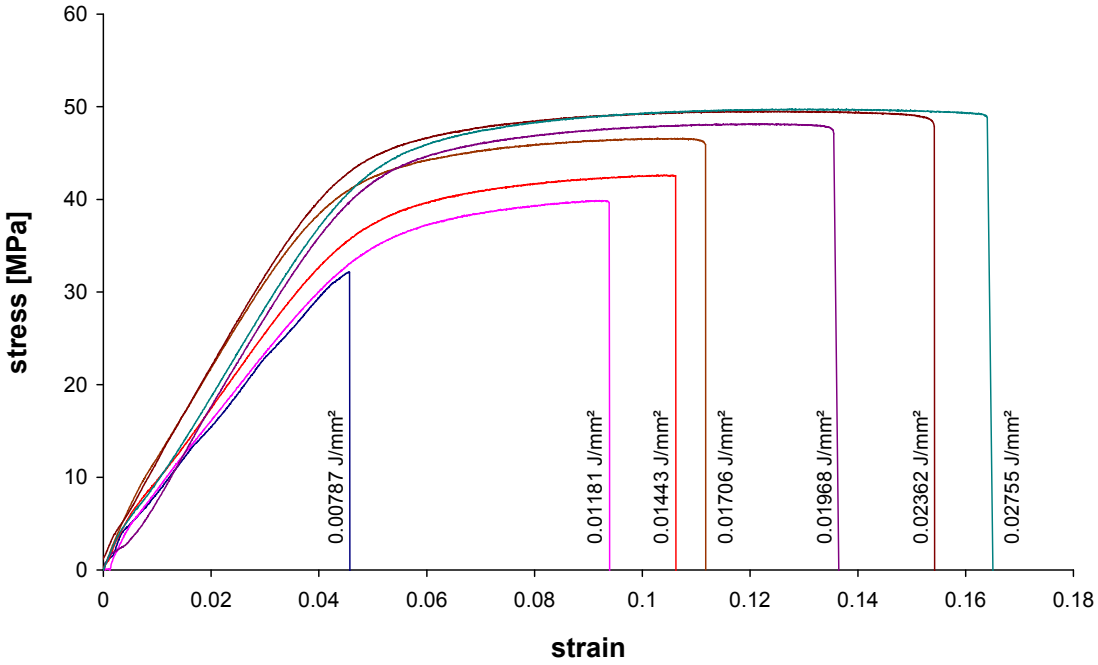


Figure 6: Stress-strain diagrams for each of the tested ED levels for the 0° orientated parts

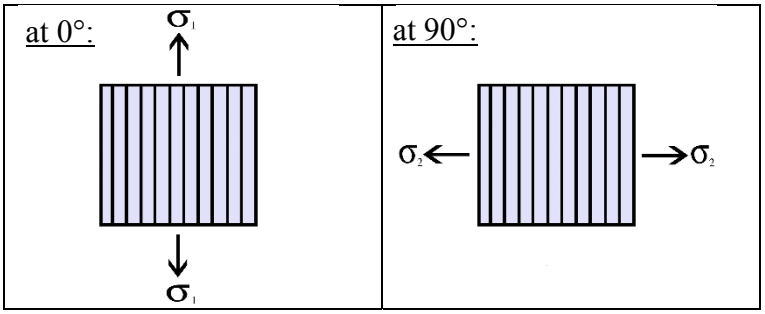


Figure 7: Uni-axial tests to find material properties

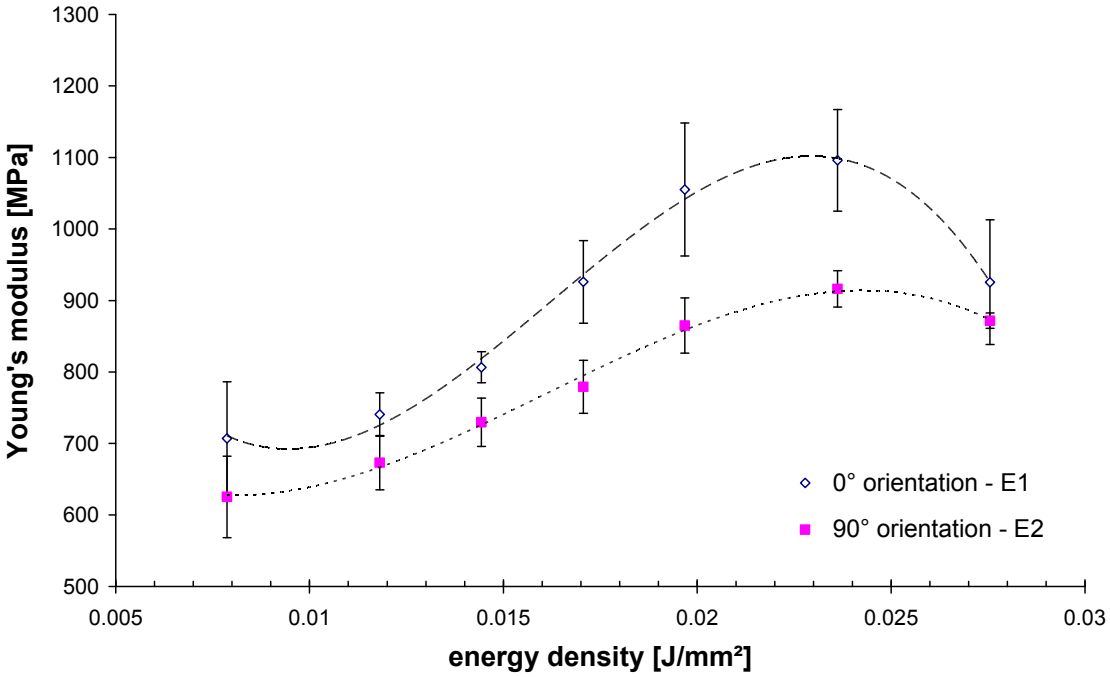


Figure 8: Young's modulus values of the test specimens. Error bars indicate the standard deviation within each set of samples.

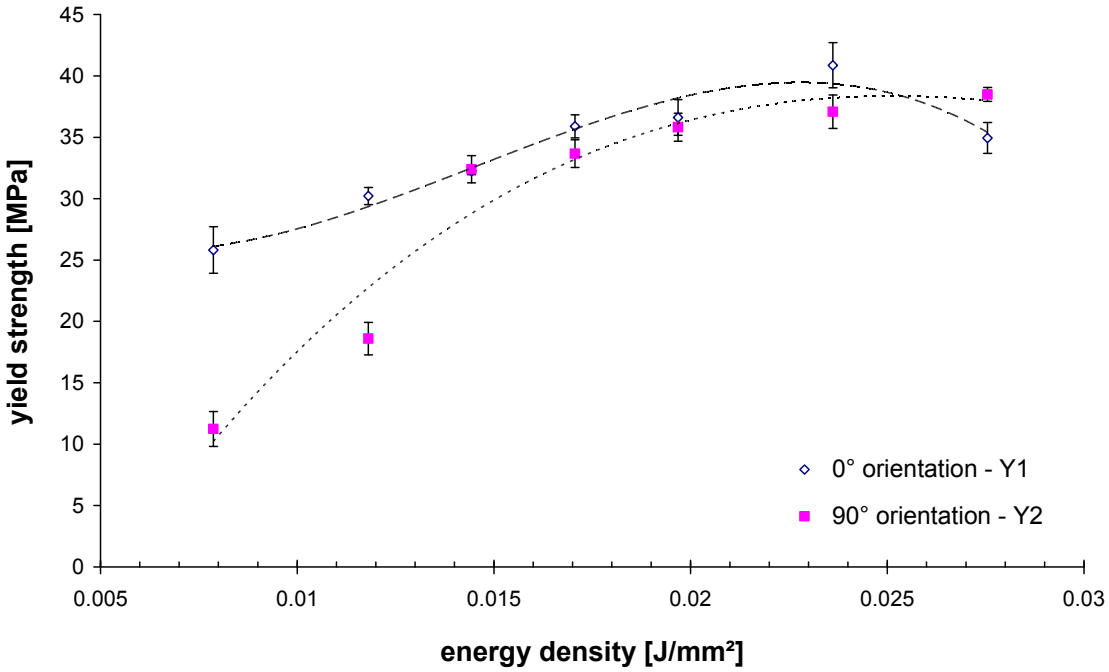


Figure 9: Yield strength values of the test specimens. Error bars indicate the standard deviation within each set of samples.

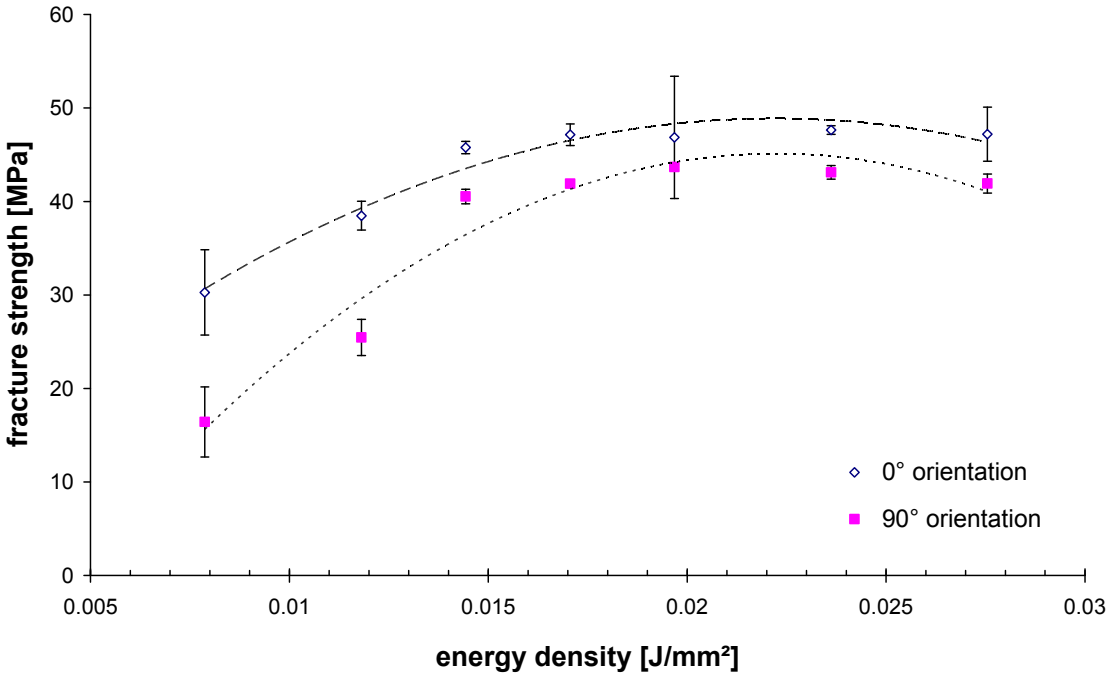


Figure 10: Fracture Strength values. Error bars indicate the standard deviation within each set of samples.

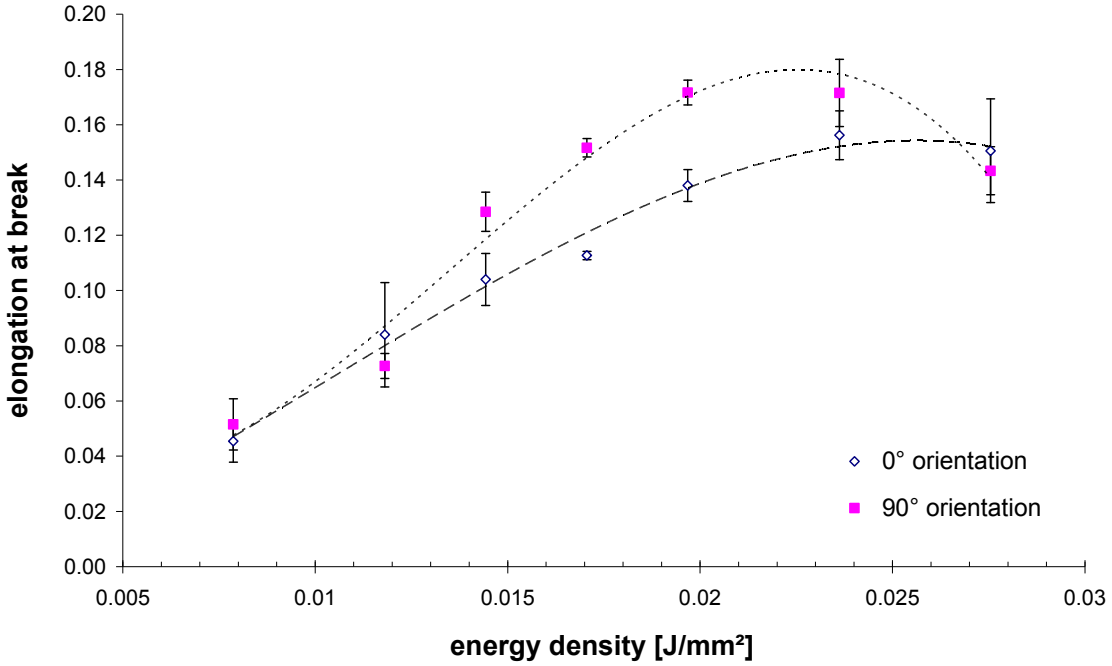


Figure 11: Elongation at Break values. Error bars indicate the standard deviation within each set of samples.

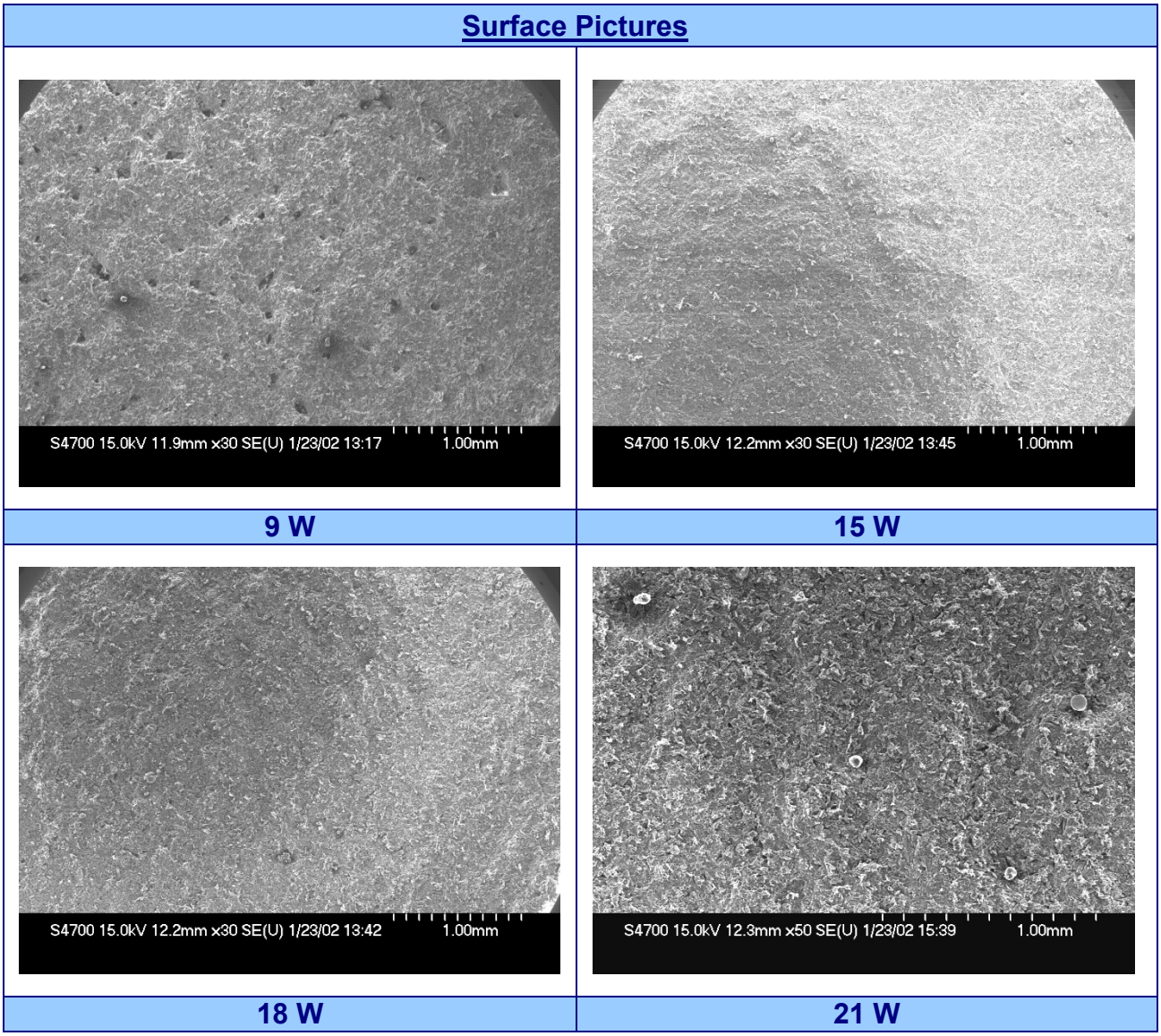


Figure 12: Surface pictures of the 0° orientated specimens (SEM Micrographs)

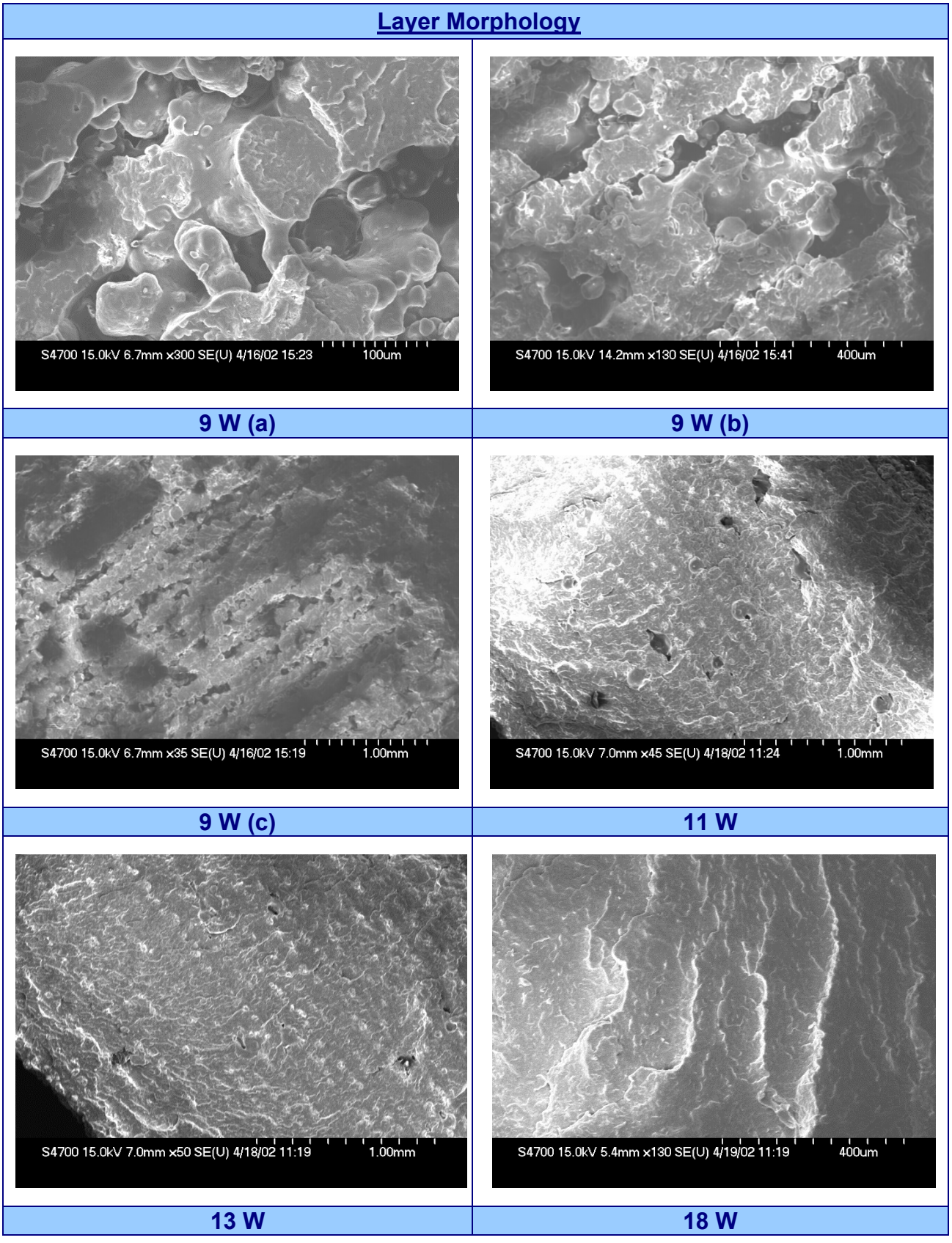


Figure 13: Close-up picture of the layers used to create the specimens (SEM Micrographs)

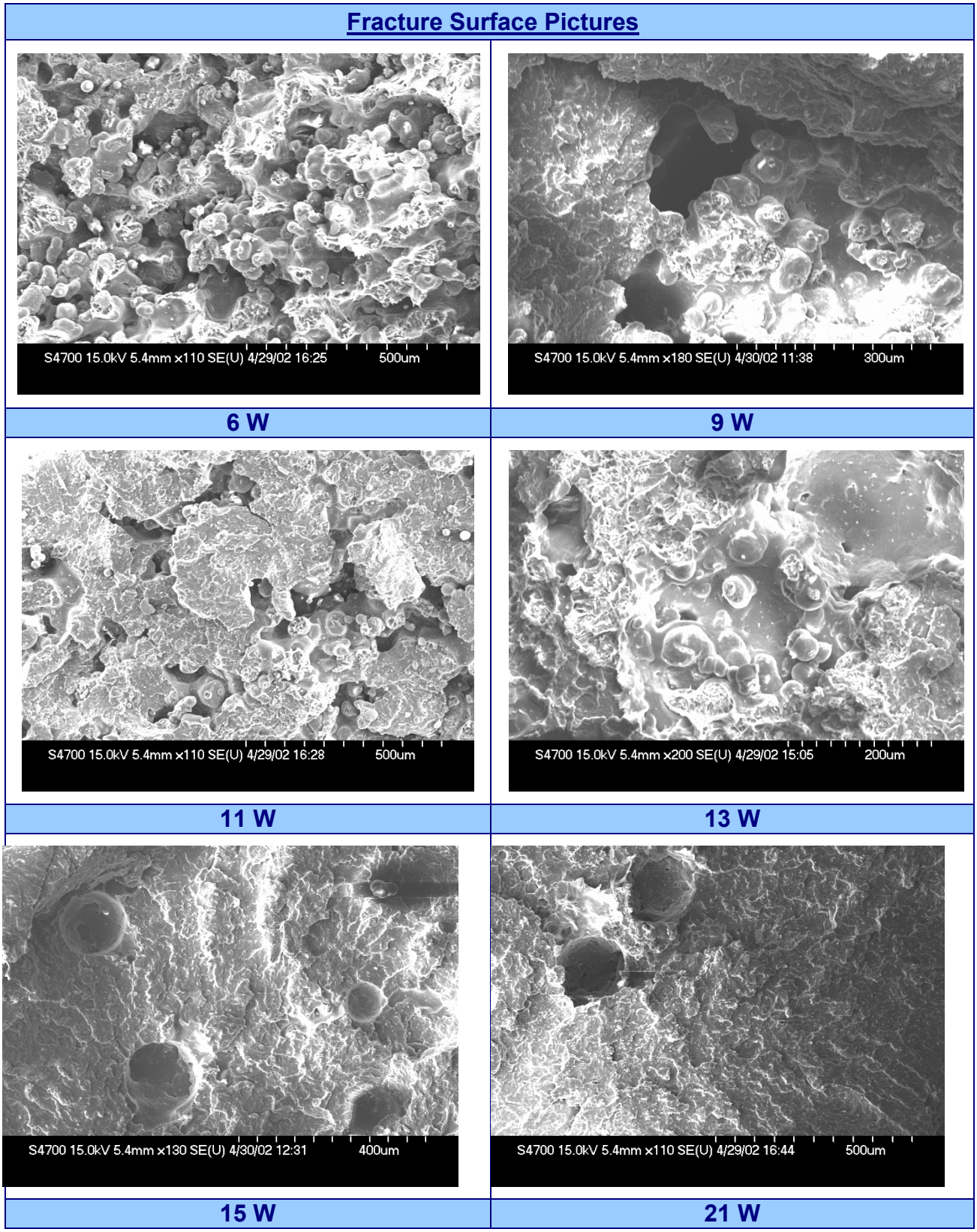


Figure 14: Fracture surface of the specimens (SEM Micrographs)

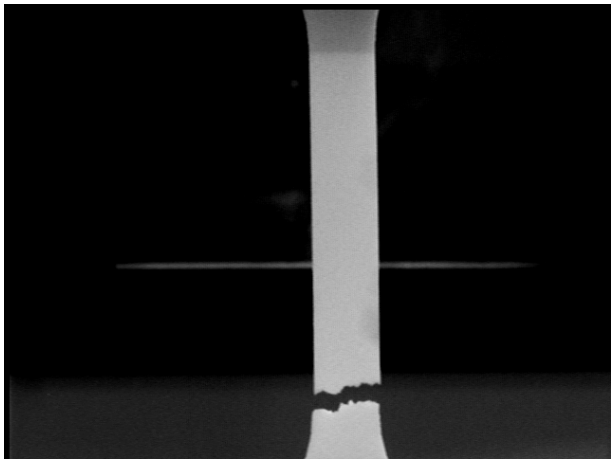

Figure 15: Fracture of the 0° orientated specimen built under an ED level of 0.00787 J/mm²

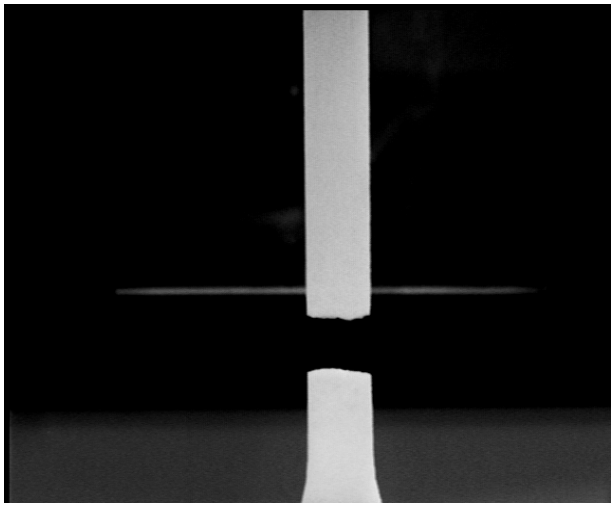

Figure 16: Fracture of the 0° orientated specimen built under an ED level of 0.01706 J/mm²

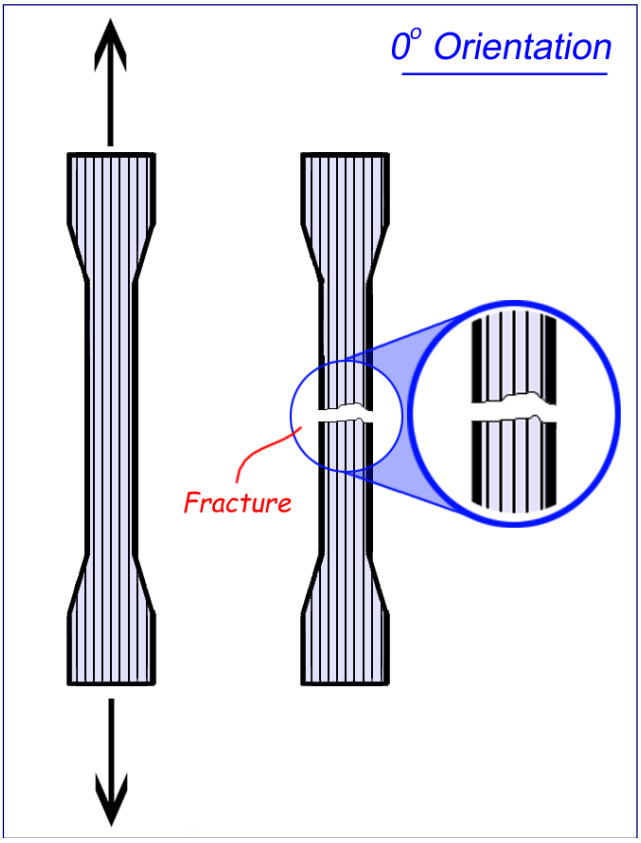


Figure 17: Predicted fracture of the 0° orientated specimens

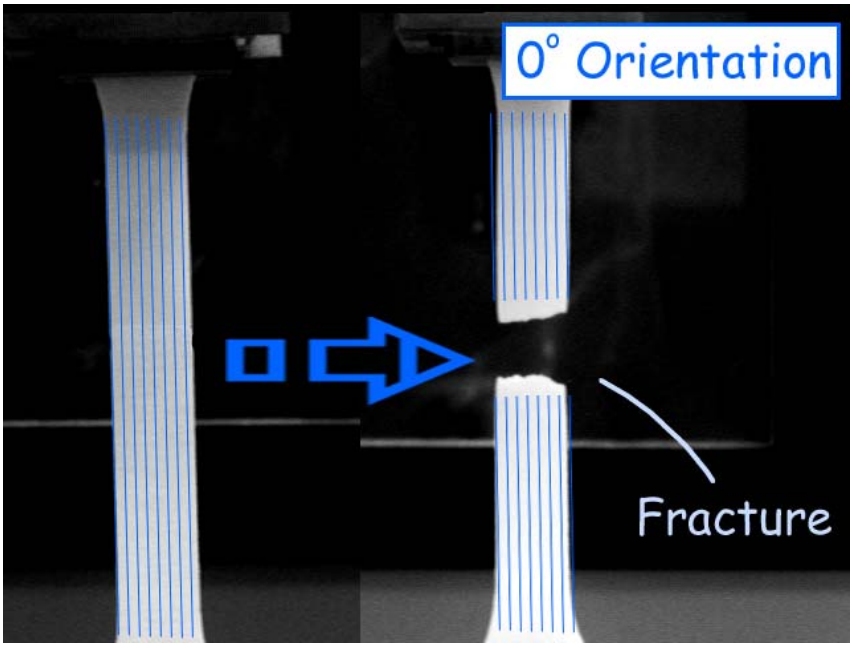


Figure 18: Actual fracture of a 0° orientated test specimen built under an ED of 0.01968 J/mm²

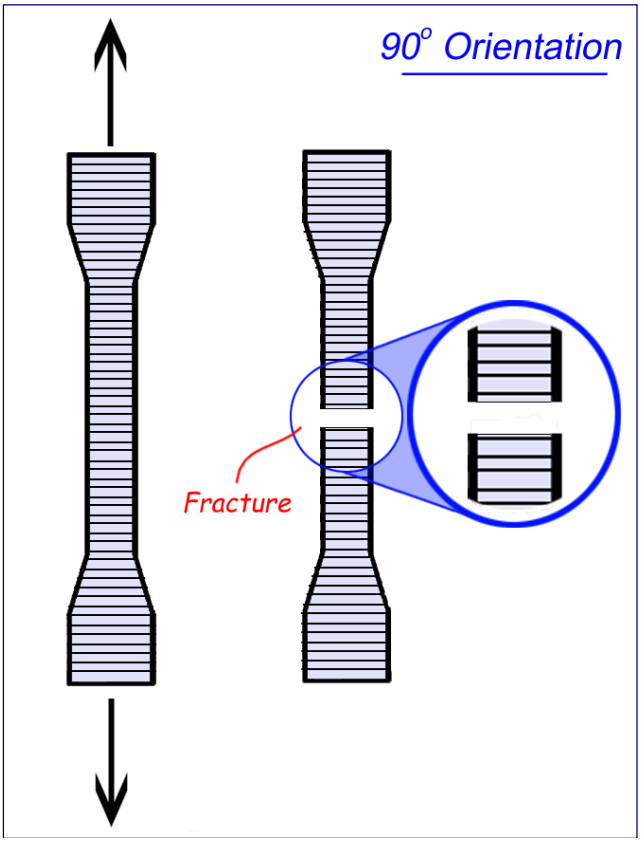


Figure 19: Predicted fracture of the 90° orientated specimens

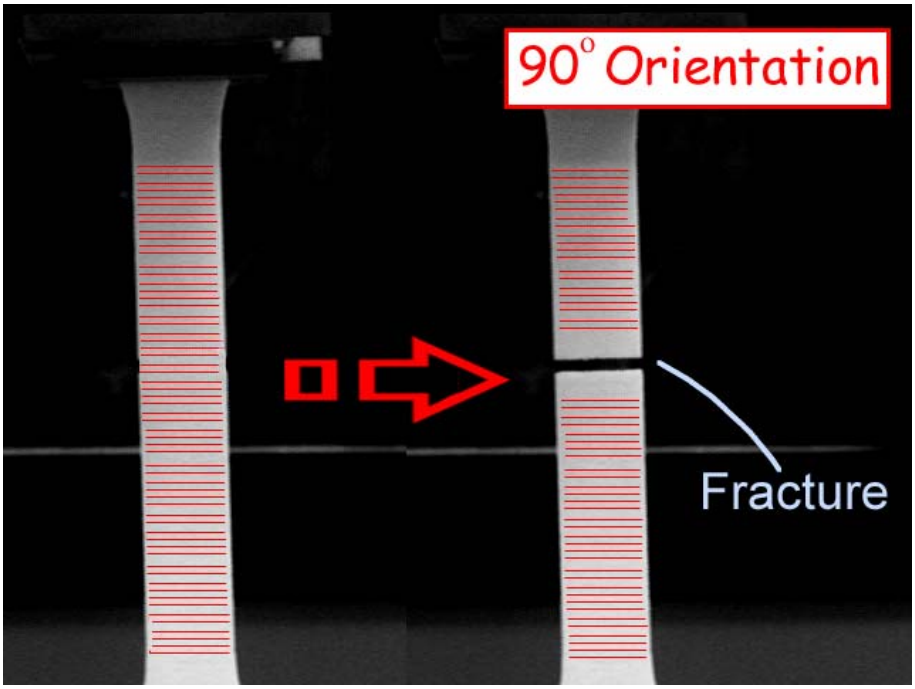


Figure 20: Actual fracture of a 90° orientated test specimen built under an ED level of 0.007754 J/mm²

Table 1: Breakdown of the parameters applied to each lot

| | Lot 1 | Lot 2 | Lot 3 | Lot 4 | Lot 5 | Lot 6 | Lot 7 |
|---|---|---|---|---|---|---|---|
| **Scan Spacing [mm]** | 0.15 | | | | | | |
| **Laser Power [W]** | 6 | 9 | 11 | 13 | 15 | 18 | 21 |
| **Energy Density [J/mm²]** | 0.00787 | 0.01181 | 0.01443 | 0.01706 | 0.01968 | 0.02362 | 0.02755 |

Table 2: Trendline equations for part width

| | |
|---|---|
| **Part Orientation 0°** | $y = -1318.9 x^2 + 68.413 x + 11.825$ |
| **Part Orientation 90°** | $y = 978.3 x^2 - 23.859 x + 12.842$ |

Table 3: Trendline equations for part thickness

| | |
|---|---|
| **Part Orientation 0°** | $y = -198113 x^3 + 8725.3 x^2 - 82.577 x + 3.2183$ |
| **Part Orientation 90°** | $y = 613.51 x^2 – 3.1147 x + 2.9594$ |

Table 4: Average cross sectional areas

| **Energy Density [J/mm²]** | **0.00787** | **0.01181** | **0.01443** | **0.01706** | **0.01968** | **0.02362** | **0.02755** |
|---|---|---|---|---|---|---|---|
| **0° Orientation** | 37.04 | 38.78 | 41.05 | 42.37 | 43.70 | 44.88 | 43.48 |
| **90° Orientation** | 37.94 | 38.20 | 38.10 | 38.78 | 40.55 | 41.88 | 42.82 |

Table 5: Trendline equations for yield strength and Young's modulus, where x represents the ED level and y represents the property value

| | |
|---|---|
| **Yield strength $Y_1$** | $y = -6 \cdot 10^6 x^3 + 265773 x^2 - 2618.6 x + 33.24$ |
| **Yield strength $Y_2$** | $y = -103179 x^2 + 5032.9 x - 22.67$ |
| **Young's Modulus $E_1$** | $y = -3 \cdot 10^8 x^3 + 2 \cdot 10^7 x^2 – 217238 x + 1578.1$ |
| **Young's Modulus $E_2$** | $y = -1 \cdot 10^8 x^3 + 7 \cdot 10^6 x^2 – 79034 x + 910.48$ |